

Magnetic-Field Tuning of Light-Induced Superconductivity in Striped $\text{La}_{2-x}\text{Ba}_x\text{CuO}_4$

D. Nicoletti^{1,*}, D. Fu¹, O. Mehio¹, S. Moore¹, A. S. Disa¹, G. D. Gu², and A. Cavalleri^{1,3}

¹ *Max Planck Institute for the Structure and Dynamics of Matter, 22761 Hamburg, Germany*

² *Condensed Matter Physics and Materials Science Department,
Brookhaven National Laboratory, Upton, New York 11973, USA*

³ *Department of Physics, Clarendon Laboratory, University of Oxford, Oxford OX1 3PU, United Kingdom*

* e-mail: daniele.nicoletti@mpsd.mpg.de

Supplemental Material

S1. Equilibrium optical response

Both $\text{La}_{2-x}\text{Ba}_x\text{CuO}_4$ (LBCO) crystals ($x = 9.5\%$ and $x = 11.5\%$) were cut and polished to give an *ac* surface with large enough area ($\sim 10 \text{ mm}^2$) to perform long-wavelength THz spectroscopy. The equilibrium optical properties at both doping levels were determined using single-cycle THz pulses generated by illuminating a photoconductive antenna with near-infrared laser pulses from a Ti:Sa amplifier. These probe pulses were focused onto the sample surface, with a $\sim 7^\circ$ incidence angle and polarization aligned perpendicular to the CuO_2 planes (along the *c* direction). The reflected electric field, $E_R(t)$, was measured by electro-optic sampling in ZnTe at different temperatures, both below and above T_C , and for various applied magnetic fields. This was then Fourier transformed to obtain the complex-valued, frequency dependent $\tilde{E}_R(\omega)$. Note that, with respect to the pump-probe measurements (see Section S2), the higher signal-to-noise ratio available for the equilibrium characterization allowed us to collect reliable data down to lower frequencies ($\sim 0.15 \text{ THz}$), thus covering the Josephson Plasma Resonance of the weakly coupled LBCO 11.5% compound.

The equilibrium reflectivity in the superconducting state, $R(\omega, T < T_C)$, was determined as $R(\omega, T < T_C) = \frac{|\tilde{E}_R(\omega, T < T_C)|^2}{|\tilde{E}_R(\omega, T \gtrsim T_C)|^2} R(\omega, T \gtrsim T_C)$. Here, $R(\omega, T \gtrsim T_C)$ is the normal-state reflectivity measured with Fourier-transform infrared spectroscopy on the same batch of samples [1], which is completely flat and featureless in the THz range. Two examples of equilibrium reflectivity spectra retrieved with this procedure are shown in Fig. S1 (blue and green circles for $x = 9.5\%$ and $x = 11.5\%$, respectively). These reflectivities were then fitted with the model that describes the optical response of a Josephson plasma (blue and green lines in Fig. S1, see Section S4 for fit model) and merged at $\omega \simeq 2.5 \text{ THz}$ with the broadband spectra from Ref. [1] (Fig. 1(c), right panel,

in main text). This allowed us to perform Kramers-Kronig transformations, thus retrieving full sets of equilibrium optical response functions (*i.e.*, complex optical conductivity $\tilde{\sigma}_0(\omega)$, complex dielectric function $\tilde{\epsilon}_0(\omega)$, complex refractive index $\tilde{n}_0(\omega)$) for all temperatures and magnetic field values investigated in our pump-probe experiment. An example of broadband equilibrium optical conductivity is reported in the inset of Fig. 1(c) in the main text.

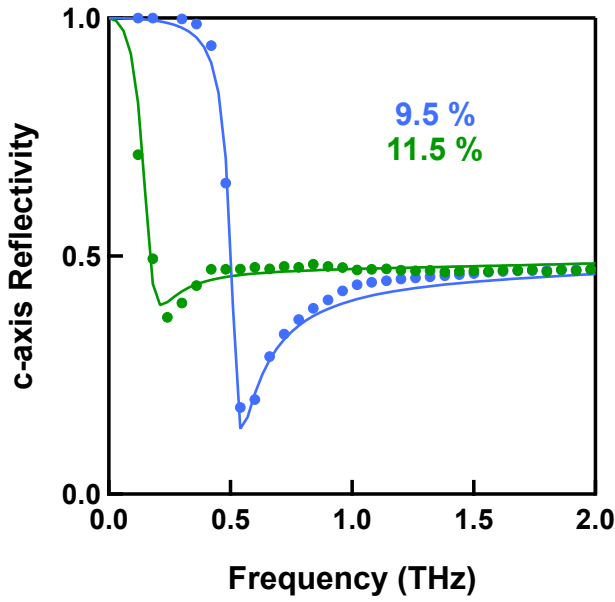


Figure S1. Equilibrium c -axis reflectivity of LBCO measured with THz time-domain spectroscopy, as described in the text. Blue and green circles are experimental data taken at $T = 5$ K (no magnetic field) on the $x = 9.5\%$ and $x = 11.5\%$ sample, respectively. Fits with a model describing the optical response of a Josephson plasma are displayed as solid lines.

S2. Evaluation of the transient optical properties

The same THz time-domain spectroscopy geometry used for the equilibrium characterization (see Section S1) was also employed to measure the transient response of the sample after photo-excitation. Optical pulses of ~ 100 fs duration and 800 nm

wavelength from the same Ti:Sa amplifier were shone at normal incidence onto the sample surface, with polarization along the c axis and a fluence of $\sim 2 \text{ mJ/cm}^2$. Delayed THz probe pulses were used to measure the pump-induced reflectivity changes for frequencies between ~ 0.3 and 2.5 THz .

The pump-induced change in the THz electric field $\Delta E_R(t, \tau) = E_R^{pumped}(t, \tau) - E_R(t)$ was acquired at each time delay τ by filtering the electro-optic sampling signal with a lock-in amplifier, triggered by modulation of the optical pump with a mechanical chopper. This measurement yielded “pump on” minus “pump off” reflected electric field.

The stationary field, $E_R(t)$, was determined for each measurement by chopping the probe beam while keeping the pump *on* at negative time delay, *i.e.* as $E_R(t, \tau \ll 0)$. Here, the pump was set to hit the sample with the same power as that used for $\Delta E_R(t, \tau)$, thus accounting for possible average heating effects.

The differential electric field $\Delta E_R(t, \tau)$ and the stationary reflected electric field $E_R(t)$ were then independently Fourier transformed to obtain the complex-valued, frequency dependent $\tilde{\Delta E}_R(\omega, \tau)$ and $\tilde{E}_R(\omega)$.

Importantly, the same measurement was repeated by (i) *directly* recording $\tilde{E}_R^{pumped}(\omega, \tau)$ and $\tilde{E}_R(\omega)$ without chopping the pump and then calculating $\Delta \tilde{E}_R(\omega, \tau) = \tilde{E}_R^{pumped}(\omega, \tau) - \tilde{E}_R(\omega)$, or by (ii) acquiring $\Delta \tilde{E}_R(\omega, \tau)$ and $\tilde{E}_R(\omega)$ simultaneously at each time delay τ by filtering the electro-optic sampling signals with two lock-in amplifiers. Method (i) does not require calibration of the absolute phase of the lock-in amplifier and eliminates phase errors in estimating the optical properties, while method (ii) avoids the introduction of possible artifacts due to long term drifts and is

particularly useful when the measured electric field contains fast-varying frequencies.

All these methods yielded identical results.

The complex reflection coefficient of the photo-excited material, $\tilde{r}(\omega, \tau)$, was determined using the relation

$$\frac{\Delta \tilde{E}_R(\omega, \tau)}{\tilde{E}_R(\omega)} = \frac{\tilde{r}(\omega, \tau) - \tilde{r}_0(\omega)}{\tilde{r}_0(\omega)}$$

To calculate these ratios, the stationary reflection coefficient $\tilde{r}_0(\omega)$ was extracted at all temperatures from the equilibrium optical properties, determined independently at the same temperature and magnetic field value (see Section S1).

These “raw” light-induced reflectivity changes were only $\sim 0.5\text{-}1\%$ and needed to be reprocessed to take into account the mismatch between the penetration depth, $d(\omega) = \frac{c}{2\omega \cdot \text{Im}[\tilde{n}_0(\omega)]}$, of the THz probe [$d(\omega \approx 0.3 - 2.5 \text{ THz}) \approx 50 - 200 \mu\text{m}$] and that of the optical pump [$d(\omega \approx 375 \text{ THz}) \approx 0.4 \mu\text{m}$]. A schematic representation of the pump-probe penetration depth mismatch is displayed in Fig. S2.

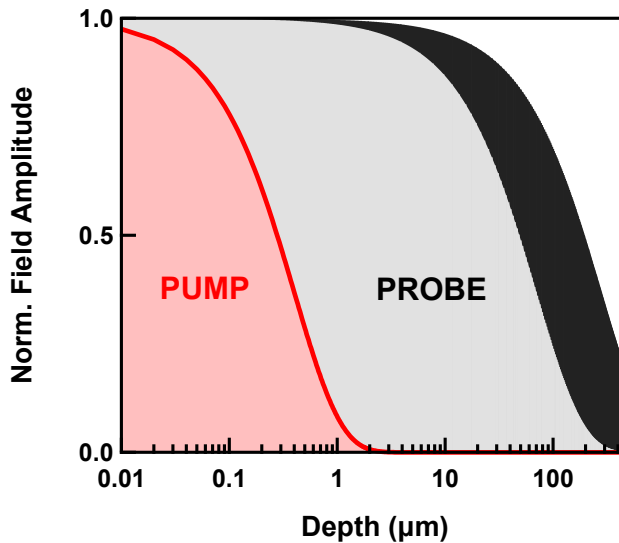


Figure S2. Schematics of pump-probe penetration depth mismatch. The exponential decay of both pump (red) and probe (black) field profiles is displayed as a function of depth into the material. The black region includes all field decay profiles within the bandwidth of the probe pulse.

This mismatch can be taken into account by modeling the response of the system as that of a homogeneously photo-excited layer of thickness $d \simeq 0.4 \mu\text{m}$ with the unperturbed bulk beneath it.

The complex reflection coefficient of such multilayer system is expressed as [2]:

$$\tilde{r}(\omega, \tau) = \frac{\tilde{r}_A(\omega, \tau) + \tilde{r}_B(\omega, \tau)e^{2i\delta(\omega, \tau)}}{1 + \tilde{r}_A(\omega, \tau)\tilde{r}_B(\omega, \tau)e^{2i\delta(\omega, \tau)}}$$

where $\tilde{r}_A(\omega, \tau)$ and $\tilde{r}_B(\omega, \tau)$ are the reflection coefficients at the interfaces vacuum/photoexcited layer and photoexcited layer/unperturbed bulk, respectively, while $\delta = 2\pi d\tilde{n}(\omega, \tau)/\lambda_0$ (here $\tilde{n}(\omega, \tau)$ is the complex refractive index of the photo-excited layer and λ_0 is the probe wavelength).

The above equation can be solved numerically, thus retrieving $\tilde{n}(\omega, \tau)$ from the experimentally determined $\tilde{r}(\omega, \tau)$, and from this the complex conductivity for a volume that is homogeneously transformed,

$$\tilde{\sigma}(\omega, \tau) = \frac{\omega}{4\pi i} [\tilde{n}(\omega, \tau)^2 - \varepsilon_\infty].$$

(here $\varepsilon_\infty = 4.5$, a standard value for high- T_C cuprates [3]).

The consistency of this multilayer model was also checked against an alternative method which treats the excited surface as a stack of thin layers with a homogeneous refractive index and describes the excitation profile by an exponential decay [4,5]. Both methods yielded very similar results.

Note that, in order to minimize the effects of pump-probe time resolution due to a finite duration of the probe pulse, we operated the delay stages in the setup as explained in Ref. [6]. Therefore, our temporal resolution is limited only by the duration of the pump pulse and by the inverse bandwidth of the probe pulse. For all measurements presented here the time resolution is of the order of 350 fs, the signal develops in $\sim 1.5 - 2$ ps, and

the relaxation occurs within $\sim 3 - 5$ ps, making any possible spectral deformation negligible [7,8].

S3. Extended data sets

In this Section we report extended data sets taken at selected pump-probe time delays, for various sample temperatures and applied magnetic fields (Fig. S3.1-6). For each set, we show three different quantities: the reflectivity, $R(\omega)$, the real conductivity, $\sigma_1(\omega)$, and the imaginary conductivity, $\sigma_2(\omega)$, of the photoexcited material. Experimental data (colored circles) are displayed along with fits performed either with a model describing the optical response of a Josephson plasma or with a Drude model for metals (colored solid lines, see also Section S4 for fitting procedure). The corresponding equilibrium spectra are also reported in each panel as gray lines.

Note that all these data and fit results have been used to produce Fig. 3 and Fig. 4 of the main text, in which we show the dynamical evolution of the interlayer phase correlation length and of the energy loss function, respectively. For this reason, we redirect the reader to the main manuscript for an extensive discussion on the experimental data.

An exception is given by the spectra of Fig. S3.5, which were taken on LBCO 11.5% at $T = 30$ K and $H = 7$ T. These data fully overlap in fact with those taken on the same material at $T = 30$ K and zero magnetic field (Fig. S3.4), and for this reason they are not reported in the main text.

The absence of any appreciable magnetic field dependence in the transient response at $T = 30$ K may relate to the fact that the equilibrium stripe order is strengthened by a magnetic field only in presence of a superconducting phase (*i.e.* for $T < T_c$ and not for $T = 30$ K). Therefore, the data of Fig. S3.5 is an additional indication that optically-

enhanced (induced) superconductivity in LBCO correlates with the strength of the equilibrium stripe order.

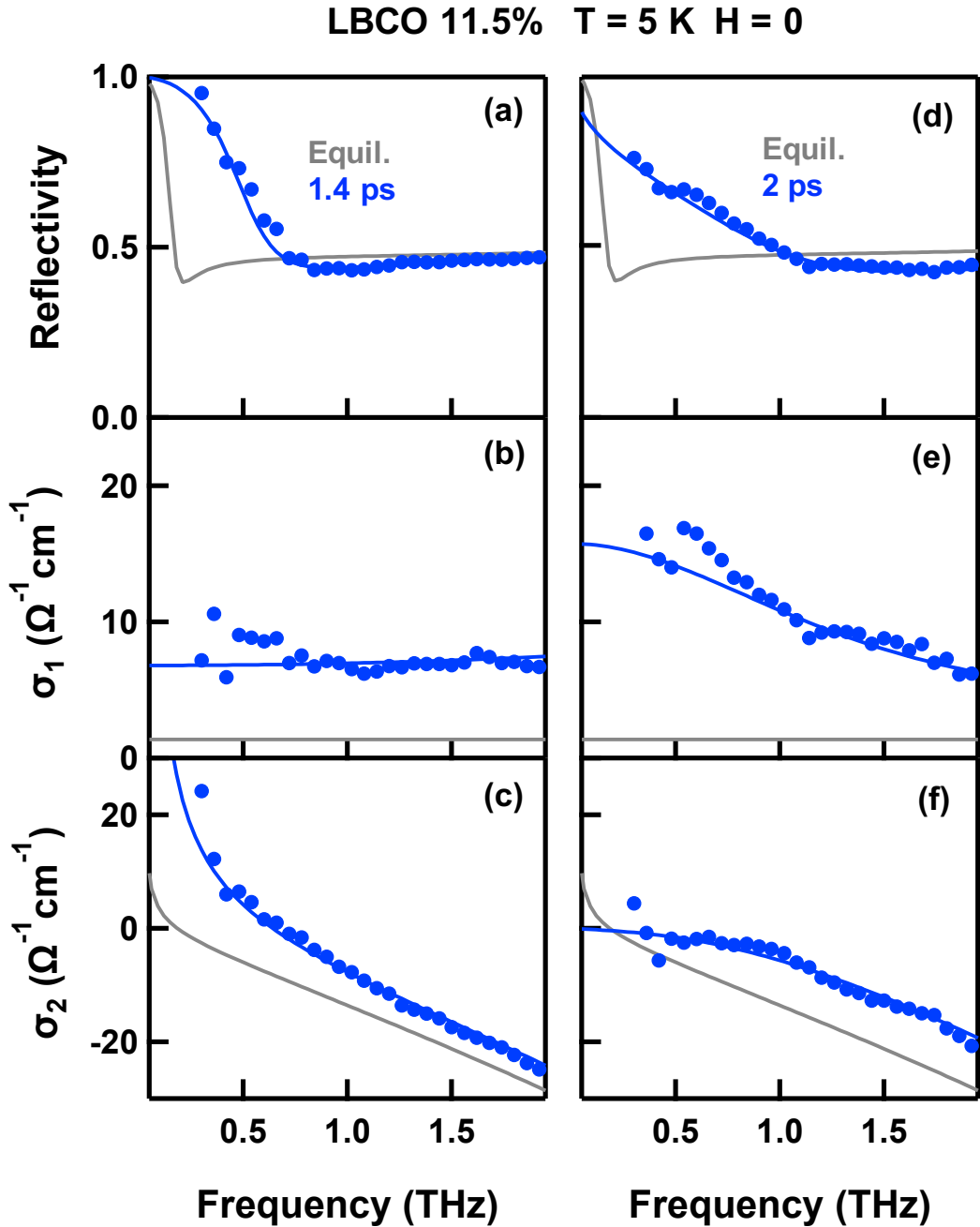


Figure S3.1. (a) c -axis THz reflectivity, (b) real, and (c) imaginary part of the optical conductivity of $\text{La}_{1.885}\text{Ba}_{0.115}\text{CuO}_4$ measured at $T = 5$ K (no magnetic field), at equilibrium (gray lines) and at $\tau = 1.4$ ps pump-probe time delay (blue circles). Fits to the transient spectra are shown as blue lines. (d,e,f) Same quantities as in (a,b,c), measured at equilibrium (gray lines) and at $\tau = 2$ ps time delay (blue). The transient data in (a,b,c) were fitted with a model describing the optical response of a Josephson plasma, while those in (d,e,f) with a Drude model for metals (see Section S4).

LBCO 11.5% T = 5 K H = 3.5 T

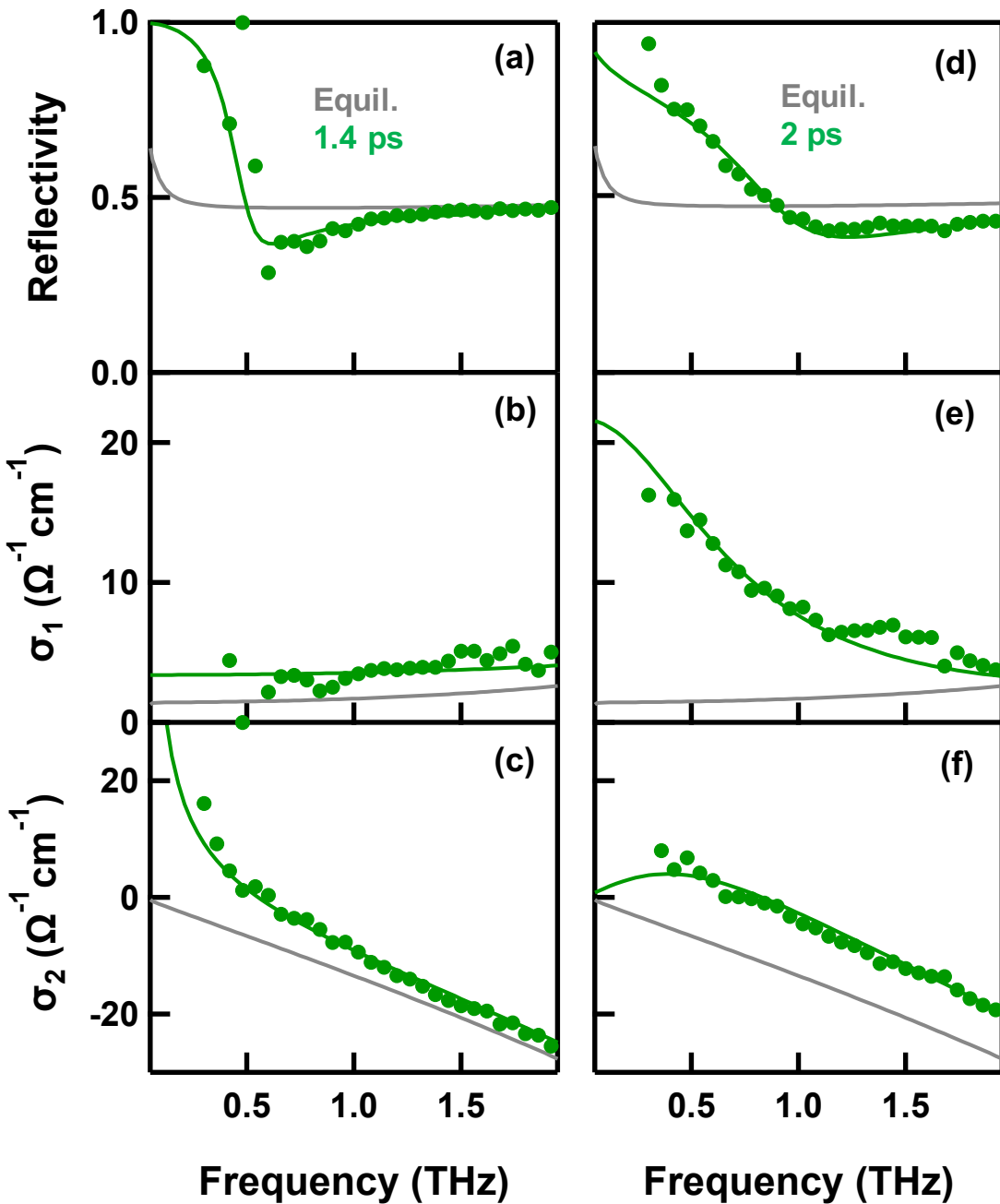


Figure S3.2. (a) c -axis THz reflectivity, (b) real, and (c) imaginary part of the optical conductivity of $\text{La}_{1.885}\text{Ba}_{0.115}\text{CuO}_4$ measured at $T = 5$ K in a 3.5 T magnetic field, at equilibrium (gray lines) and at $\tau = 1.4$ ps pump-probe time delay (green circles). Fits to the transient spectra are shown as green lines. (d,e,f) Same quantities as in (a,b,c), measured at equilibrium (gray lines) and at $\tau = 2$ ps time delay (green). The transient data in (a,b,c) were fitted with a model describing the optical response of a Josephson plasma, while those in (d,e,f) with a Drude model for metals (see Section S4).

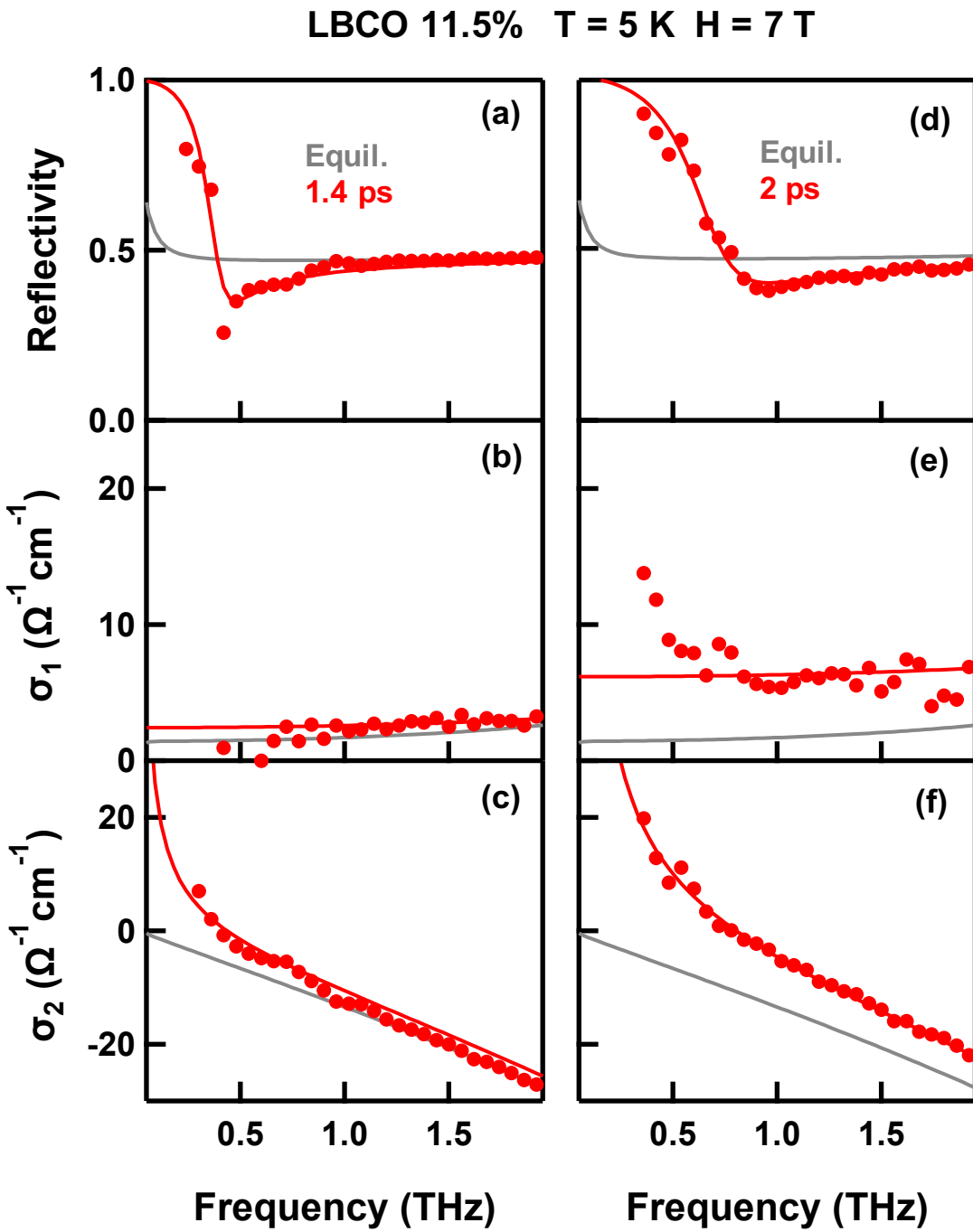


Figure S3.3. (a) c -axis THz reflectivity, (b) real, and (c) imaginary part of the optical conductivity of $\text{La}_{1.885}\text{Ba}_{0.115}\text{CuO}_4$ measured at $T = 5$ K in a 7 T magnetic field, at equilibrium (gray lines) and at $\tau = 1.4$ ps pump-probe time delay (red circles). Fits to the transient spectra are shown as red lines. (d,e,f) Same quantities as in (a,b,c), measured at equilibrium (gray lines) and at $\tau = 2$ ps time delay (red). All transient data were fitted with a model describing the optical response of a Josephson plasma (see Section S4).

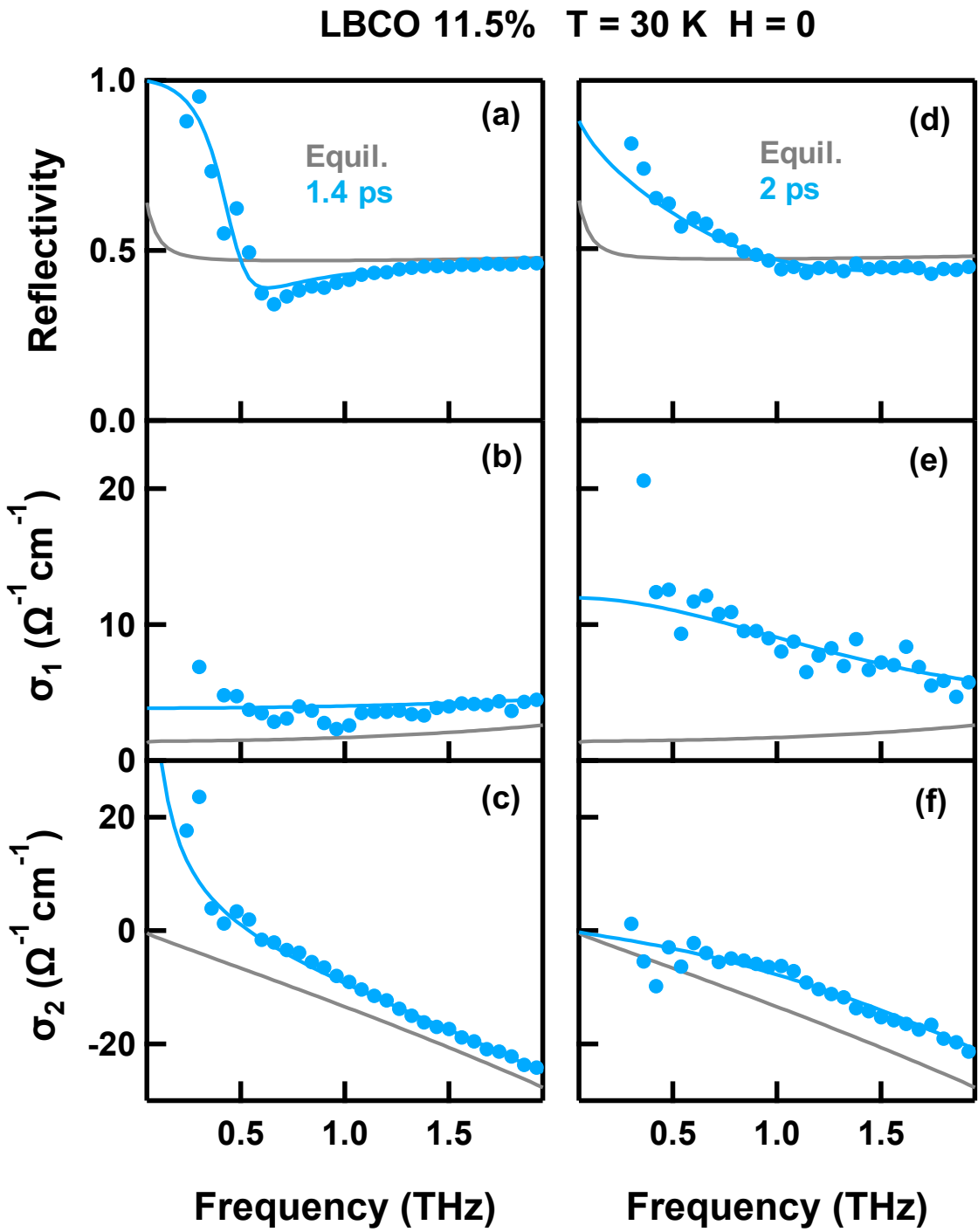


Figure S3.4. (a) c -axis THz reflectivity, (b) real, and (c) imaginary part of the optical conductivity of $\text{La}_{1.885}\text{Ba}_{0.115}\text{CuO}_4$ measured at $T = 30 \text{ K}$ (no magnetic field), at equilibrium (gray lines) and at $\tau = 1.4 \text{ ps}$ pump-probe time delay (light blue circles). Fits to the transient spectra are shown as light blue lines. (d,e,f) Same quantities as in (a,b,c), measured at equilibrium (gray lines) and at $\tau = 2 \text{ ps}$ time delay (light blue). The transient data in (a,b,c) were fitted with a model describing the optical response of a Josephson plasma, while those in (d,e,f) with a Drude model for metals (see Section S4).

LBCO 11.5% T = 30 K H = 7 T

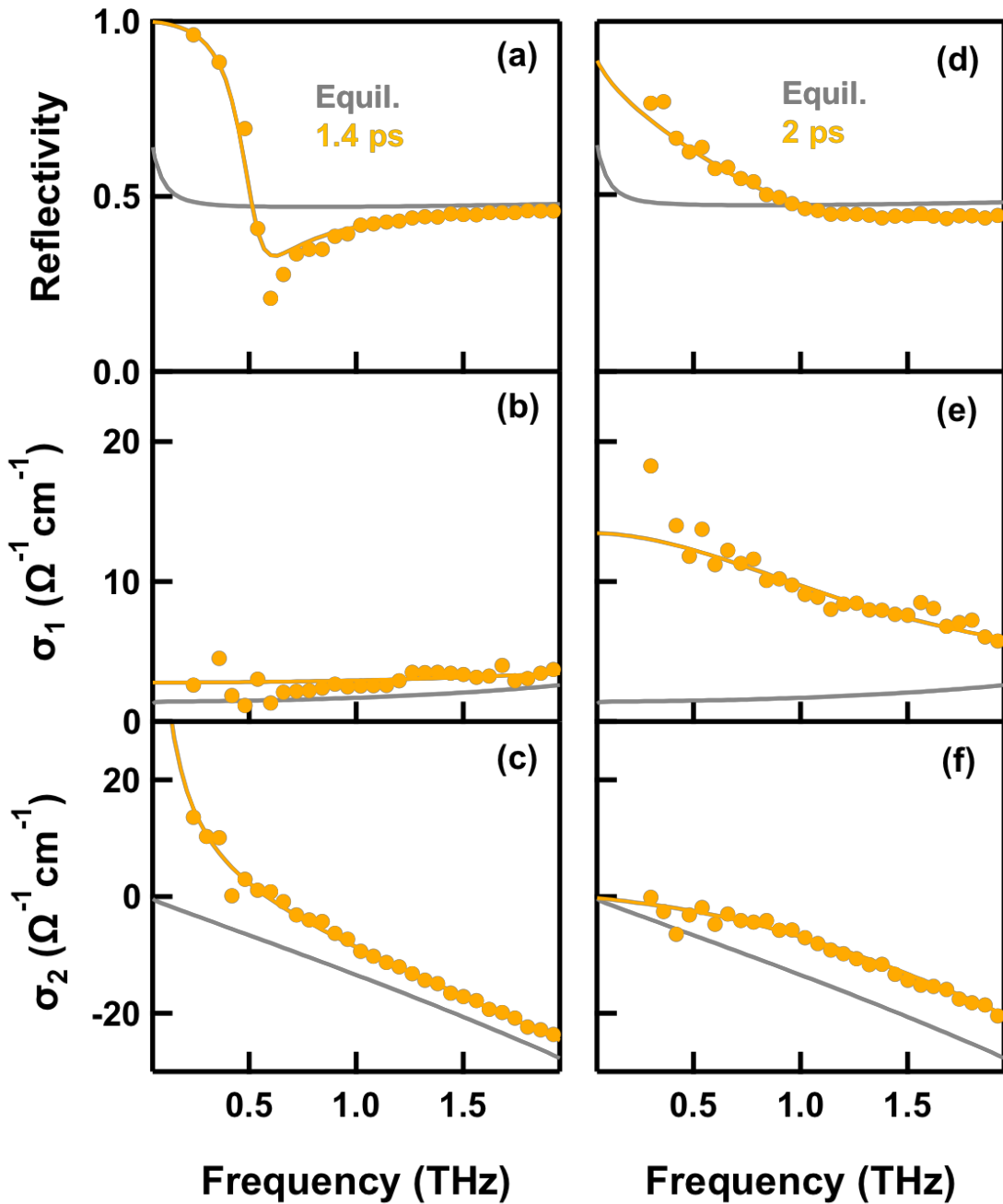


Figure S3.5. (a) c -axis THz reflectivity, (b) real, and (c) imaginary part of the optical conductivity of $\text{La}_{1.885}\text{Ba}_{0.115}\text{CuO}_4$ measured at $T = 30$ K in a 7 T magnetic field, at equilibrium (gray lines) and at $\tau = 1.4$ ps pump-probe time delay (yellow circles). Fits to the transient spectra are shown as yellow lines. (d,e,f) Same quantities as in (a,b,c), measured at equilibrium (gray lines) and at $\tau = 2$ ps time delay (light blue). The transient data in (a,b,c) were fitted with a model describing the optical response of a Josephson plasma, while those in (d,e,f) with a Drude model for metals (see Section S4).

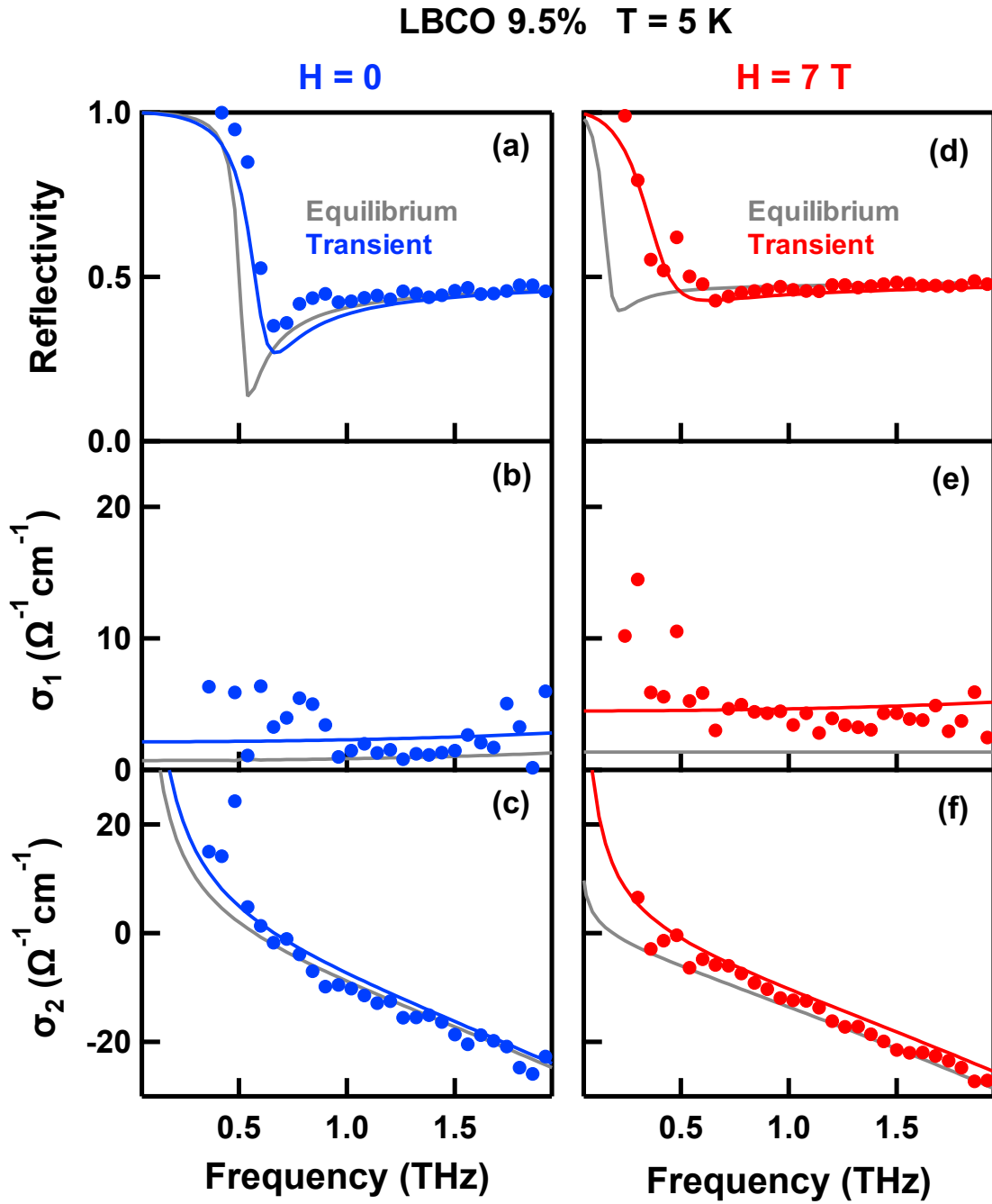


Figure S3.6. (a) c -axis THz reflectivity, (b) real, and (c) imaginary part of the optical conductivity of $\text{La}_{1.905}\text{Ba}_{0.095}\text{CuO}_4$ measured at $T = 5 \text{ K}$ (no magnetic field), at equilibrium (gray lines) and at $\tau = 1 \text{ ps}$ pump-probe time delay (blue circles). Blue lines show fits to the transient spectra with a model describing the response of a Josephson plasma. (d,e,f) Same quantities as in (a,b,c), measured in $\text{La}_{1.905}\text{Ba}_{0.095}\text{CuO}_4$ at $T = 5 \text{ K}$ in presence of a 7 T magnetic field. Transient data, taken at $\tau = 1.4 \text{ ps}$, are shown here as red circles, while fits with the Josephson plasma model as red lines.

S4. Fitting procedure

All transient optical spectra reported in this work could be satisfactorily reproduced using either a model describing the response of a Josephson Plasma or with a Drude model for metals. For each given data set (taken at a specific doping, sample temperature, magnetic field value and pump-probe time delay τ), the transient reflectivity, $R(\omega)$, the real part of the optical conductivity, $\sigma_1(\omega)$, and its imaginary part, $\sigma_2(\omega)$, were simultaneously fitted with a single set of parameters.

The phonon modes in the far- and mid-infrared spectral region ($5 \text{ THz} \lesssim \omega \lesssim 20 \text{ THz}$) and the high-frequency electronic absorption ($\omega \gtrsim 100 \text{ THz}$) were fitted from the equilibrium spectra (Fig. 1(c) of main text) with Lorentz oscillators, for which the complex dielectric function is expressed as

$$\tilde{\epsilon}_{HF}(\omega) = \sum_i \frac{S_i^2}{(\Omega_i^2 - \omega^2) - i\omega\Gamma_i},$$

and kept fixed throughout the whole analysis. Here, Ω_i , S_i , and Γ_i are central frequency, strength, and damping coefficient of the i^{th} oscillator, respectively.

The low-frequency spectral range ($\omega \lesssim 2.5 \text{ THz}$), which was directly probed in our pump-probe experiment, required the introduction of an additional term in the model. For all data taken at long time delays ($\tau \gtrsim 2 \text{ ps}$), for which the reflectivity edge appeared broadened, each set of transient optical spectra could be well reproduced by a simple Drude term (see Fig. S4(g-i)). The full complex dielectric function used in this case is expressed as

$$\tilde{\epsilon}_D(\omega) = \epsilon_\infty [1 - \omega_p^2 / (\omega^2 + i\Gamma\omega)] + \tilde{\epsilon}_{HF}(\omega)$$

where ω_p and Γ are the Drude plasma frequency and momentum relaxation rate, which were left as free parameters for the fit, while ϵ_∞ was kept fixed to 4.5, a standard value for high- T_C cuprates [3].

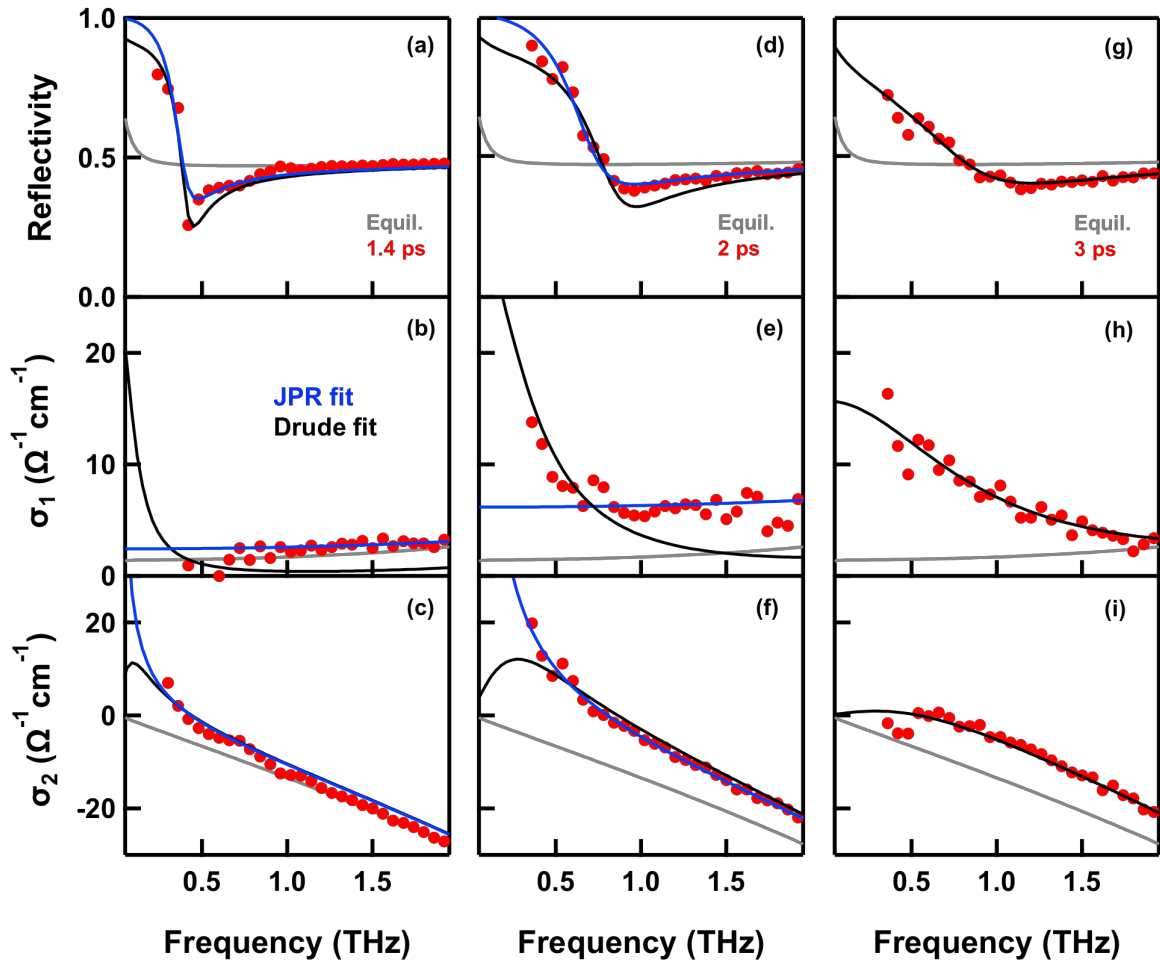


Figure S4. (a) c -axis THz reflectivity, (b) real, and (c) imaginary part of the optical conductivity of $\text{La}_{1.885}\text{Ba}_{0.115}\text{CuO}_4$ measured at $T = 5$ K in a 7 T magnetic field, at equilibrium (gray lines) and at $\tau = 1.4$ ps pump-probe time delay (red circles). Best fits to the transient spectra performed with a Josephson plasma and with a Drude model are shown as blue and black lines, respectively. (d,e,f) Same quantities as in (a,b,c), measured at equilibrium (gray lines) and at $\tau = 2$ ps time delay (red circles). (g,h,i) Same quantities as in (a,b,c), measured at equilibrium (gray lines) and at $\tau = 3$ ps time delay (red circles). Here, no Josephson plasma model was used to reproduce the data.

The transient response at earlier time delays ($\tau \lesssim 2$ ps) could also be satisfactorily reproduced by the same Drude model introduced above (black curves in Fig. S4(a-f)), although the momentum relaxation rate converged to values below the lowest probed frequency ($\Gamma < 0.3$ THz).

Alternatively, fits of at least comparable quality were performed, for these early delays, using a model describing the optical response of a Josephson Plasma at equilibrium (blue curves in Fig. S4(a-f)). Such model, which was also employed to reproduce the equilibrium spectra in the superconducting state (see Fig. S1), is able to fully capture all main features observed in the experimental data at early delays, *i.e.*, a sharp edge in $R(\omega)$, a gapped $\sigma_1(\omega)$, and a diverging $\sigma_2(\omega)$ toward low frequencies.

The full dielectric function is expressed in this case as

$$\tilde{\varepsilon}_J(\omega) = \varepsilon_\infty \left(1 - \omega_J^2/\omega^2\right) + \tilde{\varepsilon}_N(\omega) + \tilde{\varepsilon}_{HF}(\omega)$$

Here, the free fit parameters are the Josephson Plasma frequency, ω_J , and $\tilde{\varepsilon}_N(\omega)$, a weak “normal fluid” component [9] (overdamped Drude term), which was introduced to reproduce the small positive offset in $\sigma_1(\omega)$ (see Fig. S4(b,e)).

Importantly, both models discussed here consistently return optical properties compatible with a superconducting response for frequencies above $\omega \gtrsim \Gamma$, with Γ playing here the role of an inverse lifetime, $1/\tau_L$, of the transient superconducting state. This means that, within the frequency range over which the optical response of the transient state can be defined ($\omega \gtrsim \Gamma = 1/\tau_L$), a transient superconductor with lifetime τ_L and a normal conductor with momentum relaxation rate $\Gamma = 1/\tau_L$ are undistinguishable.

Despite this intrinsic ambiguity, we stress here that the evidence of a transient superconducting state in our measurement is very solid. Firstly, it should be emphasized that, starting from a weak superconductor at equilibrium (as indicated by a pre-existing Josephson Plasma Resonance, see *e.g.* Fig. 4(c) in main text), we observe a continuous transformation into a qualitatively identical phase with a blue-shifted resonance. At least for early time delays ($\tau \lesssim 2$ ps), the width of this resonance is essentially limited by our frequency resolution, returning $1/\Gamma$ values in excess of ~ 5 -

10 ps, from which one may extract carrier mobilities of at least $\sim 10^4 \text{ cm}^2/(\text{V}\cdot\text{s})$. These are extremely high values, which would be unprecedented for out-of-plane transport in a highly resistive normal state oxide [10].

Even at later time delays ($\tau \gtrsim 2 - 3 \text{ ps}$), the momentum relaxation rates returned by Drude fits, $1/\Gamma \approx 1 \text{ ps}$, are still anomalously high for conventional incoherent charge transport, and are rather suggestive of a strongly fluctuating superconducting state [11,12], which may persist for several picoseconds after photo-excitation.

Finally, the fact that such high mobility transport occurs at a density which is very close to the *c*-axis density of Cooper pairs in the same compound at equilibrium (as determined by the frequency of the plasma resonance) gives additional evidence in support of the picture of optically enhanced superconducting transport in photo-stimulated $\text{La}_{2-x}\text{Ba}_x\text{CuO}_4$.

REFERENCES (Supplemental Material)

-
- ¹ C. C. Homes, M. Hücker, Q. Li, Z. J. Xu, J. S. Wen, G. D. Gu, and J. M. Tranquada, “Determination of the optical properties of $\text{La}_{2-x}\text{Ba}_x\text{CuO}_4$ for several dopings, including the anomalous $x = 1/8$ phase”, Phys. Rev. B **85**, 134510 (2012).
- ² M. Dressel and G. Grüner, *Electrodynamics of Solids*, Cambridge University Press, Cambridge (2002).
- ³ D. van der Marel, H. J. A. Molegraaf, J. Zaanen, Z. Nussinov, F. Carbone, A. Damascelli, H. Eisaki, M. Greven, P. H. Kes, and M. Li, “Quantum critical behaviour in a high- T_c superconductor”, Nature **425**, 271 (2003).
- ⁴ M. Mitrano, A. Cantaluppi, D. Nicoletti, S. Kaiser, A. Perucchi, S. Lupi, P. Di Pietro, D. Pontiroli, M. Riccò, S. R. Clark, D. Jaksch, and A. Cavalleri, “Possible light-induced superconductivity in K_3C_60 at high temperature”, Nature **530**, 461 (2016).
- ⁵ A. Cantaluppi, M. Buzzi, G. Jotzu, D. Nicoletti, M. Mitrano, A. Perucchi, P. Di Pietro, D. Pontiroli, M. Riccò, and A. Cavalleri, “Pressure tuning of light-induced superconductivity in K_3C_60 ”, Nat. Phys. **14**, 837 (2018).
- ⁶ J. T. Kindt and C. A. Schmuttenmaer, “Theory for determination of the low-frequency time-dependent response function in liquids using time-resolved terahertz pulse spectroscopy”, J. Chem. Phys. **110**, 8589 (1999).
- ⁷ J. Orenstein and J. S. Dodge, “Terahertz time-domain spectroscopy of transient metallic and superconducting states”, Phys. Rev. B **92**, 134507 (2015).
- ⁸ D. Nicoletti, M. Mitrano, A. Cantaluppi, and A. Cavalleri, “Comment on Terahertz time-domain spectroscopy of transient metallic and superconducting states”, arXiv:1506.07846 (2015).
- ⁹ D. van der Marel and A. Tsvetkov, “Transverse optical plasmon in layered superconductors”, Czech. J. Phys. **46**, 3165 (1996).
- ¹⁰ S. Kaiser, C. R. Hunt, D. Nicoletti, W. Hu, I. Gierz, H. Y. Liu, M. Le Tacon, T. Loew, D. Haug, B. Keimer, and A. Cavalleri, “Optically induced coherent transport far above T_c in underdoped $\text{YBa}_2\text{Cu}_3\text{O}_{6+\delta}$ ”, Phys. Rev. B **89**, 184516 (2014).
- ¹¹ L. S. Bilbro, R. Valdés Aguilar, G. Logvenov, O. Pelleg, I. Bozovic, and N. P. Armitage, “Temporal correlations of superconductivity above the transition temperature in $\text{La}_{2-x}\text{Sr}_x\text{CuO}_4$ probed by terahertz spectroscopy”, Nat. Phys. **7**, 298 (2011).
- ¹² C. R. Hunt, D. Nicoletti, S. Kaiser, T. Takayama, H. Takagi, and A. Cavalleri, “Two distinct kinetic regimes for the relaxation of light-induced superconductivity in $\text{La}_{1.675}\text{Eu}_{0.2}\text{Sr}_{0.125}\text{CuO}_4$ ”, Phys. Rev. B **91**, 020505(R) (2015).